Universal Features of Collective Interactions in Hard-Sphere Systems at Higher Volume Fractions

doi: 10.1063/1.1764053

Universal Features of Collective Interactions in Hard-Sphere Systems at Higher Volume Fractions

M. Tokuyama*, Y. Terada*, H. Yamazaki† and I. Oppenheim**

*Institute of Fluid Science, Tohoku University, Sendai 980-8577, Japan
†Fuji Photo Film Co. Ltd., Nishiazabu 2-26-30, Tokyo 106-8620, Japan
**Department of Chemistry, Massachusetts Institute of Technology, Cambridge, MA 02139, USA

Abstract. In order to investigate the universal features of collective behavior due to the many-body interactions, we perform two types of computer simulations on hard-sphere systems, a Brownian-dynamics simulation on polydisperse suspensions of hard spheres, where the hydrodymamic interactions between particles are neglected, and a molecular-dynamics simulation on atomic systems of hard spheres. Thus, we show that the long-time self-diffusion coefficient in atomic systems has the same form as that derived theoretically by Tokuyama and Oppenheim (TO) for the monodisperse suspension by taking into account the many-body hydrodynamic interactions, except that the singular point is now replaced by a new one. We also show that the difference between two coefficients in both systems can be well explained by the short-time self-diffusion coefficient derived theoretically for a wide range of volume fractions.

INTRODUCTION

We consider N different hard spheres with radius a_i and mass m_i $(i = 1,...,N)$ in a cubic box of length L at a constant temperature T. We assume that the distribution of radii obeys a Gaussian distribution with the standard deviation σ divided by the average radius a and the mass m_i is proportional to a_i^3. Then, the particle volume fraction is given by $\phi_{eq} = (4\pi a^3 n_{eq}/3)(1+3\sigma^2)$, where $n_{eq} = N/L^3$. In the present paper, we discuss three different systems. The first is a suspension of monodisperse hard spheres with both hydrodynamic and direct interactions between particles. This was theoretically analyzed by Tokuyama and Oppenheim (TO) [1, 2]. The second is suspensions of monodisperse and polydisperse hard spheres without hydrodynamic interactions. The third is atomic systems of monodisperse and polydisperse hard spheres. The last two systems are investigated by computer simulations. Thus, we show that the long-time collective behavior is universal for different systems.

BASIC EQUATIONS FOR SUSPENSIONS OF HARD SPHERES

We first summarize and discuss the basic equations for a monodisperse suspension of hard spheres with $a_i = a$ and $m_i = m$, where the spheres are suspended in an equilibrium fluid with a viscosity η_0 and $\sigma = 0$. The present system has four characteristic lengths and times [1, 2]; the molecular radius r_m, the microscopic time t_m, the average moving distance of a particle $r_B(= a(t_B/t_D)^{1/2})$, the Brownian relaxation time $t_B(= m/\zeta_0)$, the screening length $\ell_H(= (6\pi a n_{eq})^{-1/2})$, within which the hydrodynamic interactions between particles become important, the screening time $t_H(= \rho a^2/\eta_0\phi)$, in which the hydrodynamic interactions become important, the particle radius a, and the structural-relaxation time $t_D(= a^2/D_0)$, which is a time required for a particle to diffuse over a distance a, where ρ is the fluid mass density, $D_0(= k_BT/\zeta_0)$ the single-particle diffusion coefficient, and $\zeta_0(= 6\pi\eta_0 a)$ the friction coefficient. In this paper we deal with concentrated suspensions in which the following inequalities hold: $r_m \ll r_B \ll \ell_H \leq a$ and $t_m \ll t_B \ll t_H \ll t_D$. Depending on the space-time scales of interest, therefore, there exist two characteristic stages. The first is a kinetic stage [K], where the space-time cutoffs (r_c, t_c), which are the minimum wavelength and time of the dynamic process of interest, are set as $r_m \ll r_c \leq \ell_H$ and $t_m \ll t_c \leq t_H$. The second is a suspension-hydrodynamic stage [SH], where $\ell_H \leq a \ll r_c$ and $t_H \ll t_c \leq t_D$.

We first review the Langevin equations in a kinetic stage [K]. Let $\boldsymbol{X}_i(t)$ and $\boldsymbol{u}_i(t)$ denote the position and the velocity of the ith particle at time t, respectively. Then, those are described by the Langevin equations discussed elsewhere [1, 2]

$$\frac{d}{dt}\boldsymbol{X}_i(t) = \boldsymbol{u}_i(t), \tag{1}$$

CP708, *Slow Dynamics in Complex Systems: 3rd International Symposium,* edited by M. Tokuyama and I. Oppenheim

$$m\frac{d}{dt}\boldsymbol{u}_i(t) = -\sum_{j=1}^{N}\boldsymbol{\zeta}(\boldsymbol{X}_{ij}(t))\cdot\boldsymbol{u}_j(t) + \sum_{j(\neq i)}\boldsymbol{F}(\boldsymbol{X}_{ij}(t)) + \boldsymbol{R}(\boldsymbol{X}_i(t),t), \quad (2)$$

where $\boldsymbol{F}(\boldsymbol{X}_{ij}(t))$ is the force between particles i and j, and $\boldsymbol{X}_{ij} = \boldsymbol{X}_i - \boldsymbol{X}_j$. Here the random force $\boldsymbol{R}(\boldsymbol{X}_i(t),t)$ obeys a Gaussian, Markov process with zero mean and satisfies

$$< \boldsymbol{R}(\boldsymbol{X}_i,t)\boldsymbol{R}(\boldsymbol{X}_j,t') >= 2k_BT\boldsymbol{\zeta}(\boldsymbol{X}_{ij})\delta(t-t'), \quad (3)$$

where the brackets $< \cdots >$ indicate an equilibrium ensemble average. The friction tensors satisfy

$$\boldsymbol{\zeta}(\boldsymbol{X}_{ij}) = \zeta_0\mathbf{1}\delta_{ij} - \sum_{k=1}^{N}\boldsymbol{\zeta}(\boldsymbol{X}_{ik})\cdot\boldsymbol{g}(\boldsymbol{X}_{kj})(1-\delta_{kj}), \quad (4)$$

where the tensors $\boldsymbol{g}(\boldsymbol{X}_{ij})$ represent the solvent-mediated hydrodynamic interactions between particles and lead to corrections to the friction coefficient ζ_0. The explicit forms of $\boldsymbol{g}(\boldsymbol{X}_{ij})$ are given, to order $(a/X_{ij})^3$, by

$$\boldsymbol{g}(\boldsymbol{X}_{ij}) = \frac{3}{4}\frac{a}{X_{ij}}(\mathbf{1}+\boldsymbol{x}_{ij}\boldsymbol{x}_{ij}), + \frac{1}{2}\left(\frac{a}{X_{ij}}\right)^3(\mathbf{1}-3\boldsymbol{x}_{ij}\boldsymbol{x}_{ij}) + O(a/X_{ij})^4, \quad (5)$$

respectively, where $\boldsymbol{x}_{ij} = \boldsymbol{X}_{ij}/X_{ij}$ and $X_{ij} = |\boldsymbol{X}_{ij}|$. The first term of Eq. (5) represents the Oseen tensor and the second the diplole tensor. Here the hydrodynamic interactions $\boldsymbol{g}(\boldsymbol{r})$ between particles can be classified into two types, depending on the range of interactions; the long-range hydrodynamic interactions between particles over a distance of order ℓ_H, which lead to divergent integrals, and the short-range hydrodynamic interactions between particles over a distance of order a. On the other hand, the force $\boldsymbol{F}(\boldsymbol{r})$ in Eq. (2) represents the direct (collision) interactions between particles over a distance of order a. Equations (1) and (2) are the basic equations to discuss the colloidal suspension of concentrated hard spheres in stage |K|. Because of the long-range interactions, however, it is beyond our capacity to deal with Eq. (2) analytically. Hence one must further reduce them to obtain a more macroscopic equation.

We now review a formal derivation of a nonlinear stochastic diffusion equation for the number density in a suspension-hydrodynamic stage |SH|. As discussed in the previous paper |2|, the relevant variable to describe the dynamics of a colloidal suspension in the stage |SH| is given by the number density

$$N(\boldsymbol{r},t) = \sum_{i=1}^{N}\Delta(\boldsymbol{X}_i(t)-\boldsymbol{r}), \quad (6)$$

where $\Delta(\boldsymbol{r})(= L^{-3}\sum_{|\boldsymbol{k}|\leq 1/r_c}\exp(-i\boldsymbol{k}\cdot\boldsymbol{r}))$ indicates the coarse-grained δ function. Taking a time derivative of $N(\boldsymbol{r},t)$ then leads to

$$\frac{\partial}{\partial t}N(\boldsymbol{r},t) = -\frac{1}{m}\nabla\cdot\boldsymbol{P}(\boldsymbol{r},t), \quad (7)$$

where the momentum density is given by $\boldsymbol{P}(\boldsymbol{r},t) = \sum_{i=1}^{N} m\boldsymbol{u}_i(t)\Delta(\boldsymbol{X}_i(t)-\boldsymbol{r})$. As discussed elsewhere |2|, in order to find a closed equation for $N(\boldsymbol{r},t)$, one further needs another equations for $\boldsymbol{P}(\boldsymbol{r},t)$ and the energy density given by $\boldsymbol{E}(\boldsymbol{r},t) = (1/2)m\sum_{i=1}^{N}\boldsymbol{u}_i(t)\boldsymbol{u}_i(t)\Delta(\boldsymbol{X}_i(t)-\boldsymbol{r})$. Taking a time derivative of those densities, using Eqs. (1) and (2), and employing a projection operator method |3| to eliminate the irrelevant processes related to the kinetic processes, such as the terms $N(\boldsymbol{r},t)\boldsymbol{R}(\boldsymbol{r},t)$ and $\boldsymbol{P}(\boldsymbol{r},t)\boldsymbol{R}(\boldsymbol{r},t)$, in an appropriate manner, one can obtain, up to lowest order in ∇,

$$\frac{\partial}{\partial t}\boldsymbol{P}(\boldsymbol{r},t) = -\frac{1}{t_B}\Big[\boldsymbol{P}(\boldsymbol{r},t) + 2t_B\nabla\cdot\boldsymbol{E}(\boldsymbol{r},t) - N(\boldsymbol{r},t)\int d\boldsymbol{r}'\Big\{\int d\boldsymbol{r}''\frac{\boldsymbol{\zeta}(\boldsymbol{r}-\boldsymbol{r}')}{\zeta_0}\cdot\boldsymbol{g}(\boldsymbol{r}'-\boldsymbol{r}'')\boldsymbol{P}(\boldsymbol{r}'') + \frac{m}{k_BT}D_0\boldsymbol{F}(\boldsymbol{r}-\boldsymbol{r}')\Big\}N(\boldsymbol{r}',t) + \boldsymbol{f}^p(\boldsymbol{r},t)\Big], \quad (8)$$

$$\frac{\partial}{\partial t}\boldsymbol{E}(\boldsymbol{r},t) = -\frac{1}{t_B}\Big[2\boldsymbol{E}(\boldsymbol{r},t) - k_BTN(\boldsymbol{r},t) + \boldsymbol{f}^e(\boldsymbol{r},t)\Big]. \quad (9)$$

Here the new random forces $\boldsymbol{f}^\alpha(\boldsymbol{r},t)(\alpha = p,e)$ satisfies

$$< \boldsymbol{f}^\alpha(\boldsymbol{r},t)\cdot\boldsymbol{f}^\beta(\boldsymbol{r}',t') >= 2D_0\delta(t-t') \times\int\frac{d\boldsymbol{r}'}{V}\frac{\boldsymbol{\zeta}(\boldsymbol{r}-\boldsymbol{r}')}{\zeta_0}\boldsymbol{A}^\alpha(\boldsymbol{r},t)\cdot\boldsymbol{A}^\beta(\boldsymbol{r}',t), \quad (10)$$

where $\boldsymbol{A}^p(\boldsymbol{r},t) = N(\boldsymbol{r},t)\mathbf{1}$ and $\boldsymbol{A}^e(\boldsymbol{r},t) = \boldsymbol{P}(\boldsymbol{r},t)$. We note here that Eqs. (8) and (9) contains two types of interactions, the hydrodynamic interactions through $\boldsymbol{g}(\boldsymbol{r})$ and the direct interactions through $\boldsymbol{F}(\boldsymbol{r})$.

In order to solve Eqs. (8) and (9) for $N(\boldsymbol{r},t)$ self-consistently, one may first use two types of expansions, the expansion in the spatial gradient $\nabla(\propto a/r_c)$ and the expansion in the slowness parameter $\partial/\partial t(\propto t_B/t_c)$ |2, 4|. In fact, we find that on the time scale of order t_D, $\partial\boldsymbol{P}(\boldsymbol{r},t)/\partial t = \partial\boldsymbol{E}(\boldsymbol{r},t)/\partial t \simeq \mathbf{0}$. Then, one may further apply the projector method again for a reduced equation for $N(\boldsymbol{r},t)$ to eliminate the irrelevant processes. After a long calculation, one can finally obtain a nonlinear stochastic equation for the local volume fraction given by $\Phi(\boldsymbol{r},t)(= 4\pi a^3N(\boldsymbol{r},t)/3)$, up to order ∇^2, |4|

$$\frac{\partial}{\partial t}\Phi(\boldsymbol{r},t) = \nabla\cdot\Big[D_S^L(\Phi(\boldsymbol{r},t))\nabla\Phi(\boldsymbol{r},t)\Big] + \boldsymbol{\xi}(\boldsymbol{r},t), \quad (11)$$

where $\boldsymbol{\xi}(\boldsymbol{r},t)$ denotes the Gaussian, Markov random force (see Ref. [4] for details). Here the long-time self diffusion coefficient $D_S^L(\Phi)$ is given by [1, 2]

$$D_S^L(\Phi) = D_S^S(\Phi)\frac{1-\frac{9}{32}\Phi}{1+(\frac{\Phi D_S^S}{\phi_g^{TO}D_0})\left(1-\frac{\Phi}{\phi_g^{TO}}\right)^{-\gamma}}, \quad (12)$$

where $\gamma = 2$ here. Here D_S^S is the short-time self-diffusion coefficient given by [1]

$$D_S^S(\Phi) = D_0/[1+h(\Phi)] \quad (13)$$

with the non-memory (short-time) hydrodynamic effect

$$h(\Phi) = \frac{2A^2}{1-A} - \frac{B}{1+2B} - \frac{AB(2+B)}{(1+B)(1-A+B)}, \quad (14)$$

where $A = \sqrt{9\Phi/8}$ and $B = 11\Phi/16$. The factor $(9\Phi/32)$ in Eq. (12) represents the coupling effect between the direct interactions and the hydrodynamic interactions, while it reduces to 2Φ for binary collisions without the hydrodynamic interactions. Here ϕ_g^{TO} is the theoretical glass transition volume fraction given by

$$\phi_g^{TO} = (4/3)^3/(7\ln 3 - 8\ln 2 + 2) \approx 0.57184\cdots. \quad (15)$$

We note here that the singular term in the denominator of Eq. (12) results from the many-body, long-range hydrodynamic interactions through the Oseen tensor. Hence the diffusion coefficient $D_S^L(\Phi(\boldsymbol{r},t))$ becomes smaller and smaller near ϕ_g^{TO} as time goes on since $D_S^L(\phi_g^{TO}) = 0$. This is the so-called dynamic anomaly.

Equation (11) is a starting equation to describe the dynamics of diffusion processes in colloidal suspensions at higher volume fractions. It enables us to describe not only the dynamics of spatial heterogeneities but also the dynamics of density fluctuations near the glass transition. It can be solved in two cases, a nonequilibrium case and an equilibrium case, separately. This is discussed next.

Let decompose $\Phi(\boldsymbol{r},t)$ into an average part $\phi(\boldsymbol{r},t)$ and a fluctiating part $\delta\phi(\boldsymbol{r},t)$; $\Phi(\boldsymbol{r},t) = \phi(\boldsymbol{r},t) + \delta\phi(\boldsymbol{r},t)$. Here $\overline{\delta\phi(\boldsymbol{r},t)} = 0$, where the bar denotes the average over an appropriate initial ensemble. Then, $\phi(\boldsymbol{r},t) \neq \phi_{eq}$ for a nonequilibrium case and $\phi(\boldsymbol{r},t) = \phi_{eq}$ for an equilibrium case. This decomposition is essential since the relative magnitude of the density fluctuation to the average density is small even near the colloidal glass transition, $|\delta\phi(\boldsymbol{r},t)/\phi(\boldsymbol{r},t)| \ll 1$. This is because the glass transition is not a critical phenomenon since there exist no correlation length diverging even at the glass transition point.

In a nonequilibrium case where $\phi(\boldsymbol{r},t) \neq \phi_{eq}$, one can decompose Eq. (11) into the nonlinear deterministic diffusion equation for $\phi(\boldsymbol{r},t)$

$$\frac{\partial}{\partial t}\phi(\boldsymbol{r},t) = \nabla\cdot\left[D_S^L(\phi(\boldsymbol{r},t))\nabla\phi(\boldsymbol{r},t)\right], \quad (16)$$

and the linear stochastic diffusion equation for $\delta\phi(\boldsymbol{r},t)$

$$\frac{\partial}{\partial t}\delta\phi(\boldsymbol{r},t) = \nabla^2\left[D_S^L(\phi(\boldsymbol{r},t))\delta\phi(\boldsymbol{r},t)\right] + \boldsymbol{\xi}(\boldsymbol{r},t). \quad (17)$$

The dynamics of spatial heterogeneities is described by the solution of Eq. (16). On the other hand, the density fluctuations are described by Eq. (17) and are observed through the self-intermediate scattering function given by $F_s(k,t) = \int d\boldsymbol{r}\exp(i\boldsymbol{k}\cdot\boldsymbol{r}) < \delta\phi(\boldsymbol{r},t)\delta\phi(\boldsymbol{0},0) > /(4\pi a^3/3)^2$.

In order to solve Eq. (16) numerically, one must fix the values of two parameters, ϕ_{eq} and z_0, as the initial conditions. Here z_0 measures how the system is spatially nonuniform initially and is given by

$$z_0 = 1 - \frac{1}{L^3}\int d\boldsymbol{r}\left|1 - \frac{\phi(\boldsymbol{r},t=0)}{\phi_{eq}}\right|, \quad (18)$$

where $z_0 = 1.0$ in an equilibrium state. Starting from nonequilibrium random configurations, the smoothing process of $\phi(\boldsymbol{r},t)$ starts to occur, leading to the equilibrium volume fraction ϕ_{eq} for long times of order $t_L(= a^2/D_S^L(\phi_{eq}))$. As discussed in Ref. [5], there exist four characteristic time stages near the glass transition. The first is the early stage where $t \ll t_\gamma(= a^2/D_S^S(\phi_{eq}))$. The spatial configurations are random and are described by $\phi(\boldsymbol{r},t) = \exp[tD_S^S\nabla^2]\phi(\boldsymbol{r},0)$. The density fluctuations are described by Eq. (17) and obeys the exponential decay $F_S(k,t) = \exp[-k^2D_S^St]$. After this stage, the finite-sized, glassy domains with $\phi(\boldsymbol{r},t) \geq \phi_g^{TO}$ are formed for $\phi_\beta \leq \phi_{eq} < \phi_g^{TO}$, where ϕ_β indicates the crossover volume fraction [5]. The smoothing process of $\phi(\boldsymbol{r},t)$ is then slowing down due to those domains. On the time scale of order t_β, therefore, those glassy domains affect the dynamics of the density fluctuations. This is the so-called β-relaxation stage where $t_\gamma \ll t \leq t_\alpha$, where t_α denotes the α-relaxation time. Depending on the time scale, the scattering function $F_S(k,t)$ obeys two types of power-law decays. In the fast β-relaxation stage where $t_\gamma \ll t \leq t_\beta$, small aggregates of glassy domains are formed and influence the dynamics of the density fluctuations, leading to the critical decay

$$F_s(k,t) = f_0 - f_1(t/t_\beta)^{b'}, \quad (19)$$

where $b'(0 < b' < 1)$ is an exponent to be dertermined, t_β the β-relaxation time, and f_i a positive constant. This decay continues up to the time scale of order t_β. In the slow β-relaxation stage $(t_\beta \leq t \leq t_\alpha)$, the aggregates grow to the larger clusters and lead to the power-law decay of von Schweidler type

$$F_s(k,t) = f_2 - f_3(t/t_\beta)^b, \quad (20)$$

where $b(0 < b < 1)$ is an exponent to be dertermined. After this stage, the glassy domains further grow to larger

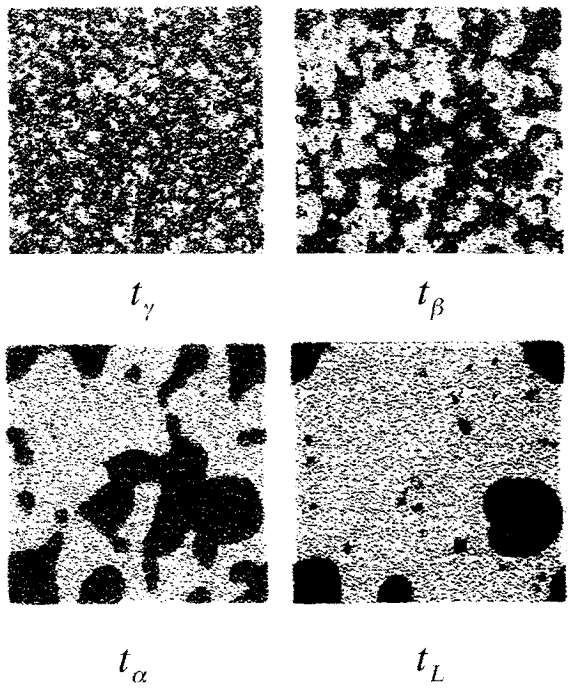

FIGURE 1. Snapshots of nonequilibrium configurations $\phi(\boldsymbol{r},t)$ in a $x-y$ plane for times $t_\gamma/t_D \simeq 4, t_\beta/t_D \simeq 800, t_\alpha/t_D \simeq 2\times 10^4$, and $t_L/t_D \simeq 4\times 10^5$ at $\phi_{eq}=0.566$ and $z_0=0.8$. The glassy regions with $\phi(\boldsymbol{r},t) \geq \phi_g^{TO}$ are colored black, while the liquid regions are colored white.

clusters and affect the dynamics of the density fluctuations, leading to the stretched exponential decay of Kohlrausch-Williams-Watts type

$$F_s(k.t) = f_4 \exp[-(t/t_\alpha)^\beta], \tag{21}$$

where $\beta(0<\beta<1)$ is a stretched exponent to be derermined. This is the so-called α-relaxation stage ($t_\alpha \leq t \leq t_L$). Here we note that the α-relaxation time t_α satisfies $t_\alpha \propto |1-\phi_{eq}/\phi_g^{TO}|^{-\eta}$, where $\eta=\gamma/\beta$. After this stage, the glassy domains disappear very slowly and the system gradually reaches the equilibrium state on the time scale of order t_L. Then, the spatial configurations become random and the density fluctuations obey the exponential decay $F_S(k,t)=\exp[-k^2 D_S^L t]$. The time exponents are listed in Table 1. In Fig. 1, the snapshot of the long-lived spatial heterogeneities is shown. The long-lived glassy clusters are shown to exist near ϕ_g^{TO} [5]. Figure 2 shows the numerical solution of Eq. (17).

In an equilibrium case where $\phi(\boldsymbol{r},t)=\phi_{eq}$, one can expand Eq. (11) in powers of $|\delta\phi/\phi_{eq}|$ near ϕ_g^{TO} and obtain the nonlinear stochastic diffusion equation for

TABLE 1. Time exponents for $\phi_{eq}=0.566$ at $k=1.3a$.

	b'	b	β	η
nonequilibrium ($z_0=0.8$)	0.37	0.72	0.59	3.41
equilibrium ($z_0=1.0$)	—	0.97	0.95	2.1

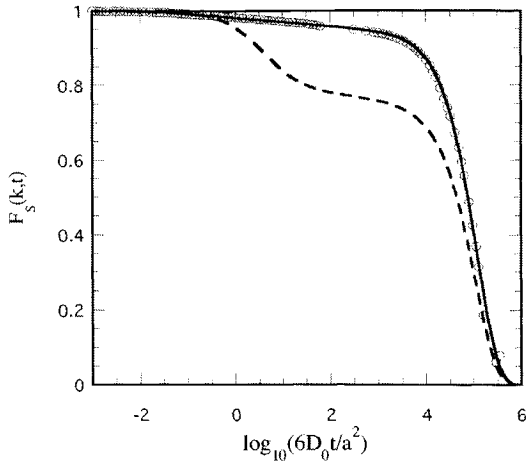

FIGURE 2. $F_S(k.t)$ versus time for $\phi_{eq}=0.566$ at $k=1.3a$. The dashed line indicates the nonequilibrium solution of Eq. (17) and the solid line the equilibrium solution given by Eq. (26). The symbols indicate the experimental data from Ref. [6]

$\delta\phi(\boldsymbol{r},t)$, up to order $|\delta\phi/\phi_{eq}|^3$, [4]

$$\begin{aligned}\frac{\partial}{\partial t}\delta\phi(\boldsymbol{r},t) &= \nabla^2\Big[D_S^L(\phi_{eq})\delta\phi(\boldsymbol{r},t) \\ &+ D_S^S(\phi_{eq})\Big\{-\omega(\phi_{eq})\delta\phi(\boldsymbol{r},t)^2 \\ &+ \kappa(\phi_{eq})\delta\phi(\boldsymbol{r},t)^3\Big]+\xi(\boldsymbol{r},t),\end{aligned} \tag{22}$$

where the random force $\xi(\boldsymbol{r},t)$ satisfies

$$\begin{aligned}&<\xi(\boldsymbol{r},t)\xi(\boldsymbol{r}',t')>=2\delta(t-t')\phi_{eq}D_S^L(\phi_{eq}) \\ &\times\nabla\cdot\nabla'\left[\tfrac{4\pi}{3}a^3\delta(t-t')+\phi_{eq}\{g(|\boldsymbol{r}-\boldsymbol{r}'|)-1\}\right].\end{aligned} \tag{23}$$

Here $g(r)$ represents the radial distribution function and the coefficients ω and κ are known smooth functions of ϕ_{eq}. Since $g(r)$ is not known, Eq. (22) must be calculated self-consistently.

In contrast to the nonequilibrium case, the long-lived spatial heterogeneities are caused by nonlinear fluctuations. Although they lead to a distinct two-step relaxation, only the glassy domains related to the α-relaxation process seem to survive because the small domains related to the β-relaxation process are easily destroyed by

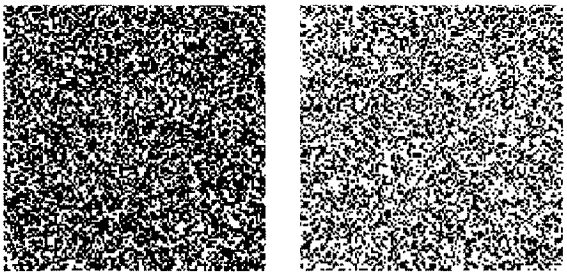

FIGURE 3. Snapshots of the density fluctuations, projected onto a $x-y$ plane, for different volume fractions. The glassy domains are clored black and the liquid domains are white.

fluctuations. In a nonequilibrium case, the clusters are stable for the fluctuations. This difference is clearly seen in Table 1.

Because the radial distribution function $g(r)$ is not known, it is rather difficult to calculate Eq.(22) numerically. In Fig. 3 the snapshots of the density fluctuations are shown for the special case where $g(r)$ is assumed to be one. Near the glass transition, the nonlinear fluctuations play an important role, forming the clusters of glassy domains, while away from the glass transition only the linear fluctuations exist, causing random configurations. In suspensions, the self-intermediate scattering function $F_S(k,t)$ can be written as $F_S(k,t) = \exp[-k^2 M_2(t)/6]$ [7], where $M_2(t)$ denotes the mean-square displacement given by

$$M_2(t) = \frac{1}{N}\sum_{i=1}^{N} < [\boldsymbol{X}_i(t) - \boldsymbol{X}_i(0)]^2 > . \qquad (24)$$

Instead of solving Eq. (22), therefore, one can derive a mean-field nonlinear equation for $M_2(t)$ [8]

$$\frac{d}{dt}M_2(t) = 6D_S^L(\phi_{eq}) + 6[D_S^S(\phi_{eq}) - D_S^L(\phi_{eq})]e^{-\lambda M_2(t)}, \qquad (25)$$

where $\lambda(\phi_{eq})$ is a free parameter to be determined from the fitting with experimental data. Equation (25) can be easily solved to give

$$M_2(t) = \frac{1}{\lambda}\ln\left[1 + \frac{D_S^S}{D_S^L}\left\{e^{t/t_\beta} - 1\right\}\right], \qquad (26)$$

where $t_\beta = 1/(6\lambda D_S^L)$. For short times $t \ll t_0 (= 1/(6\lambda D_S^S))$, Eq. (26) reduces to $M_2(t) \simeq 6D_S^S t$, leading to the exponential decay $F_S(k,t) = \exp[-k^2 D_S^S t]$. In the fast β-relaxation stage where $t_0 \le t \le t_\beta$, the scattering function obeys the logarithmic decay

$$F_s(k,t) = g_0 - g_1 \ln(D_0 t/a^2), \qquad (27)$$

where $g_0 = (1 + t_D/t_0)^{-a_k}$ and $g_1 = a_k g_0/(1 + t_0/t_D)$. Here $a_k = k^2/(6\lambda)$. In the slow β-relaxation stage where $t_\beta \le t \le t_\alpha$, it obeys the power-law decay of von Schweidler type

$$F_s(k,t) = (1 + t/t_0)^{-a_k} - g_2(t/t_\beta)^b, \qquad (28)$$

where g_2 is a positive constant. In the α-relaxation stage where $t_\alpha \le t \le t_L$, it obeys the stretched exponential decay of Kohlrausch-Williams-Watts type

$$F_s(k,t) = (1 + t/t_0)^{-a_k}\exp[-(t/t_\alpha)^\beta]. \qquad (29)$$

The time exponents are listed in Table1. After this stage, the scattering function obeys the exponential decay $F_S(k,t) = \exp[-k^2 D_S^L t]$, where $M_2(t) \simeq 6D_S^L t$.

Both in a nonequilibrium case and in an equilibrium case, the finite-sized, long-lived clusters are considered to be the origin of well-known two-step relaxation. Once the diffusion coefficient $D_S^L(\Phi)$ is given in the form of Eq. (12), Eq.(11) is shown to describe the characteristic features observed by experiments near the glass transition very well. Although the diffusion coefficient given by Eq. (12) mainly results from the many-body, long-range hydrodynamic interactions, that singular form is considered to be rather universal even for different many-body interactions. We next discuss this.

COMPUTER SIMULATIONS ON HARD-SPHERE SYSTEMS

In this section we investigate how the form of the self-diffusion coefficent given by Eq. (12) is universal even for different interactions. As discussed in the previous papers [9, 10], we consider two kinds of hard-sphere systems, the suspension of hard spheres and the atomic system of hard spheres, and perform two types of computer simulations, a Brownian-dynamics (BD) simulation on polydisperse suspensions and a molecular-dynamics (MD) simulation on atomic systems. In the following, we thus test whether the following form of the diffusion coefficient holds or not:

$$\frac{D_S^{L(p)}(\phi_{eq})}{d_p} = \frac{\mu(\phi_{eq})}{D_0}\frac{1 - \nu(\phi_{eq})}{1 + (\frac{D_S^S}{D_0})(\frac{\phi_{eq}}{\phi_c})\left(1 - \frac{\phi_{eq}}{\phi_c(\sigma)}\right)^{-\gamma}}, \qquad (30)$$

where $\mu(\phi_{eq})$ is a function of ϕ_{eq}, and D_S^S is given by Eq. (13). Here γ is an exponent to be determined and $\phi_c(\sigma)$ the singular point to be determined. For the suspensions of neutral colloids, TO theory finds that $\mu = D_S^S$, $\nu = 9\phi_{eq}/32$, and $\phi_c = \phi_g^{TO}$. The coefficient d_p comes from the fact that the position vector and the time for the suspension ($p = S$) and those for the atomic system ($p =$

A) are scaled by different parameters from each other. In fact, we have $d_p = D_0$ in the suspension, while $d_p = d_0(= av_0)$ in the atomic system, where $v_0 = \sqrt{dk_BT/m}$ denotes the average velocity of an atom. Here we note that in both simulations $\nu = 0$ since there is no coupling between the hydrodynamic interactions and collisions.

We first discuss the suspensions. For simplicity, we neglect the hydrodynamic interactions between particles because it is not easy to treat the Oseen tensor numerically. Hence the system contains mainly two kinds of interactions; the direct interaction between particles and the interaction between a particle and solvent particles. In a kinetic stage of the polydisperse suspensions, the velocity $\boldsymbol{u}_i(t)$ of ith sphere then obeys the Langevin equation

$$m\frac{d}{dt}\boldsymbol{u}_i(t) = -\zeta_i\boldsymbol{u}_i(t) + \sum_{j(\neq i)} \boldsymbol{F}(\boldsymbol{X}_{ij}(t)) + \boldsymbol{R}_i(t), \quad (31)$$

where $\zeta_i = 6\pi\eta a_i$ and the Gaussian random force $\boldsymbol{R}_i(t)$ satisfies

$$< \boldsymbol{R}_i(t)\boldsymbol{R}_j(t') >= 2k_BT\zeta_i\delta_{ij}\delta(t-t')\mathbf{1}. \quad (32)$$

Since $d\boldsymbol{u}_i(t)/dt \simeq 0$ on a time scale of order t_D, use of Eq.(31) leads to

$$\frac{d}{dt}\boldsymbol{X}_i(t) = \frac{1}{\zeta_i}\sum_{j\neq i}\boldsymbol{F}(\boldsymbol{X}_{ij}(t)) + \boldsymbol{\xi}_i(t). \quad (33)$$

Here the reduced random force $\boldsymbol{\xi}_i(t)(= \boldsymbol{R}_i(t)/\zeta_i)$ satisfies

$$< \boldsymbol{\xi}_i(t)\boldsymbol{\xi}_j(t') >= 2D_{0i}\delta(t-t')\delta_{i,j}\mathbf{1}, \quad (34)$$

where $D_{0i} = k_BT/\zeta_i$. In order to calculate Eq. (33) numerically, we first scale the position vector $\boldsymbol{X}_i$ with radius a, time with t_D, radius a_i with a, and D_S^L with D_0. Then, we employ the forward Euler difference scheme to integrate Eq. (33) with time step 10^{-3} under periodic boundary and appropriate initial conditions together with the momentum and the energy conservation laws, where elastic binary collisions between particles are assumed and the total number of particles N is chosen to be 10976. The simulation results are compared with Eq.(26).

Since the above system of suspensions lacks one of important interactions, that is, hydrodynamic interactions, we still need to investigate the system which contains complete mechanisms. It is an atomic system of hard spheres, where only the direct interactions between particles play an important role. In the atomic systems, the velocity $\boldsymbol{u}_i(t)$ of ith particle obeys the Newton equation

$$m_i\frac{d}{dt}\boldsymbol{u}_i(t) = \sum_{j\neq i}\boldsymbol{F}(\boldsymbol{X}_{ij}(t)). \quad (35)$$

Before we solve Eq.(35) numerically under the same initial and boundary conditions as those in BD, we also scale the position vector $\boldsymbol{X}_i$ with radius a, the velocity $\boldsymbol{u}_i(t)$ with v_0, time t with $t_0(= a/v_0)$, mass m_i with m, and D_S^L with d_0. Similar to Eq. (25), $M_2(t)$ is described by the mean-field equation [9]

$$\frac{d}{dt}M_2(t) = 2dD_S^L + 2d\left[\frac{v_0^2}{d}t - D_s^L\right]e^{-\lambda M_2(t)}, \quad (36)$$

which is easily solve to give

$$M_2(t) = \frac{1}{\lambda}\ln\left[1 + 2\left(\frac{t_\beta}{t_A}\right)^2\{e^{t/t_\beta} - (1 + t/t_\beta)\}\right], \quad (37)$$

where $t_A = 1/(v_0\lambda^{1/2})$ denotes the short time for an atom to move over a distance of order $\lambda^{-1/2}$. The simulation results are compared with Eq.(37).

Both simulations, MD and BD, are done for two cases separately, a monodisperse case where spheres are all identical, that is, $a_i = a$, $m_i = m$, and $\sigma = 0$, and a polydisperse case, where $\sigma = 0.06$ here. In both simulations, we start from two kinds of non-equilibrium initial states. One is a disordered initial state [D] which shows a random configuration obtained by using the Jodrey and Tory's algorithm [11]. The other is an ordered initial state [O] which shows a face-centered-cubic configuration. Then, we wait for a long time enough to reach a final state in which the mean-square displacement grows linearly in time. We then use this final state as an initial state and repeat the simulations again, until the whole time behavior of the mean-square displacement coincides with a previous one. Depending on the values of the volume fractions, there are three phase regions; a fluid region for $0 < \phi < \phi_f(\sigma)$, a metastable region for $\phi_f(\sigma) \leq \phi < \phi_m(\sigma)$, and a crystal region for $\phi_m(\sigma) \leq \phi$, where $\phi_f(\sigma)$ and $\phi_m(\sigma)$ are the so-called freezing and melting volume fractions, respectively. From our simulations, we thus find $\phi_f(0) \simeq 0.51$, $\phi_f(0.06) \simeq 0.53$, $\phi_m(0) \simeq 0.54$, and $\phi_m(0.06) \simeq 0.57$.

In Figs. 4 and 5, the mean-square displacement $M_2(t)$ is shown in an equilibrium liquid state. Both simulation results are shown to be in good agreement with the mean-field solutions given by Eqs. (26) and (37). We note here that the mean-square displacement satisfies the following asymptotic solutions:$M_2(t) \simeq 6D_0t$ for $t \leq t_D$ and $6D_S^Lt$ for $t_D \ll t$ in suspensions, and $M_2(t) \simeq (v_0t)^2$ for $t \leq t_0$ and $6D_S^Lt$ for $t_0 \ll t$ in atomic systems. The short-time behavior in both systems are different from each other since in suspensions it is governed by the short-time diffusion process, while in atomic systems it is governed by the ballistic motion. Thus, we find the long-time self-diffusion coefficients $D_S^{L(p)}(\phi)/d_p$ for different volume fractions, where $d_p = d_0$ for atomic systems and $d_p = D_0$ for suspensions. In Fig. 6, we plot the long-time self-diffusion coefficient $D_S^{L(p)}(\phi_{eq})/d_p$ versus ϕ_{eq}. Then, we

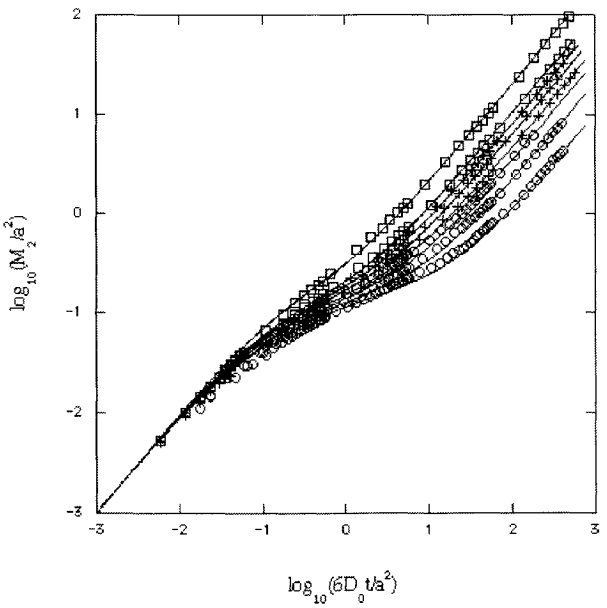

FIGURE 4. A log-log plot of the mean-square displacement $M_2(t)$ for suspensions versus time for different volume fractions (from left to right) 0.45, 0.50, 0.51, 0.52, 0.53, 0.54, 0.55, 0.56. The solid lines indicate the mean-field results given by Eq. (26). The symbols indicate the BD results: the open squares are for a monodisperse equilibrium fluid state, the crosses are for a monodisperse metastable fluid state, and the open circles are for a polydisperse metastable fluid state.

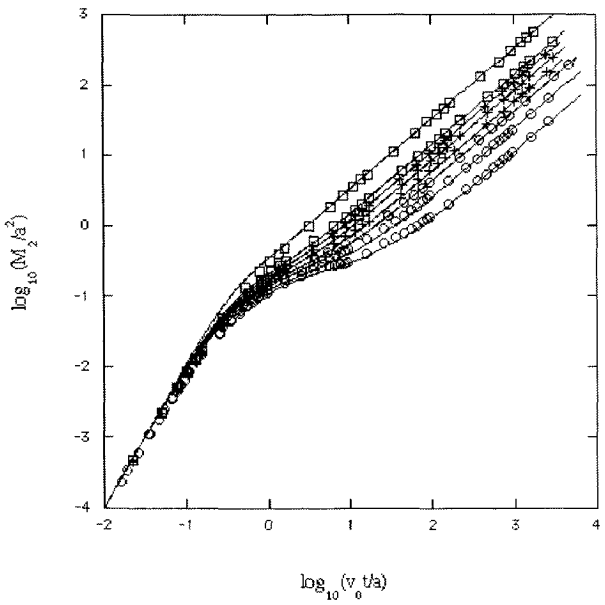

FIGURE 5. A log-log plot of the mean-square displacement $M_2(t)$ for atomic systems versus time. The solid lines indicate the mean-field results given by Eq. (36). The details are the same as in Fig. 4.

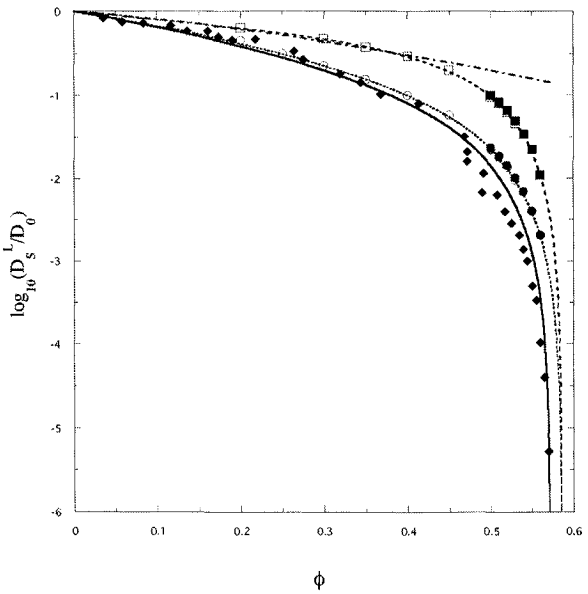

FIGURE 6. A log plot of the long-time self-diffusion coefficient $D_S^{L(p)}(\phi)/d_p$ versus ϕ. The open symbols indicate the simulation results for a monodisperse case; the squares for $D_S^{L(C)}/D_0$ and the circles for $D_S^{L(A)}/d_0$. The filled symbols indicate those for a polydisperse case. The solid line is the theoretical results given by Eqs. (12). The dotted and dashed lines indicate the diffusion coefficients $D_S^{L(A)}/d_0$ and $D_S^{L(C)}/D_0$ given by Eq. (30), respectively. The filled diamonds indicate the experimental data from Ref. [6].

TABLE 2. Coefficients and exponents.

	γ	μ	ν	ϕ_c
BD ($\sigma = 0$)	2.0	D_0	0	0.586
BD ($\sigma = 0.06$)	2.0	D_0	0	0.586
MD ($\sigma = 0$)	2.0	D_S^S	0	0.586
MD ($\sigma = 0.06$)	2.0	D_S^S	0	0.586
TO ($\sigma = 0$)	2.0	D_S^S	$\frac{9}{32}\phi_{eq}$	ϕ_g^{TO}

show that the simulation results are described by Eq. (30) very well if the coefficents μ, ν, the exponent γ, and the singular point ϕ_c are set as in Table 2. Here we note that the singular point $\phi_c(\sigma)$ is not a sensitive function of σ. In fact, Doliwa and Heuer [12] have also found by a Monte-Carlo simulation that $\phi_c(0.1) \simeq 0.587$. In the simulations $\mu = D_0$ comes from the fact that the systems do not contain the hydrodynamic interactions, while in the atomic systems $\mu = D_S^S$ comes from the fact that the systems contain the full mechanisms. In order to check whether this is correct or not, we also plot the short-time self-diffusion coefficient $D_S^S(\phi)$ versus ϕ in Fig. 7. For comparison, the experimental data are also shown. The simulation results are shown to agree with

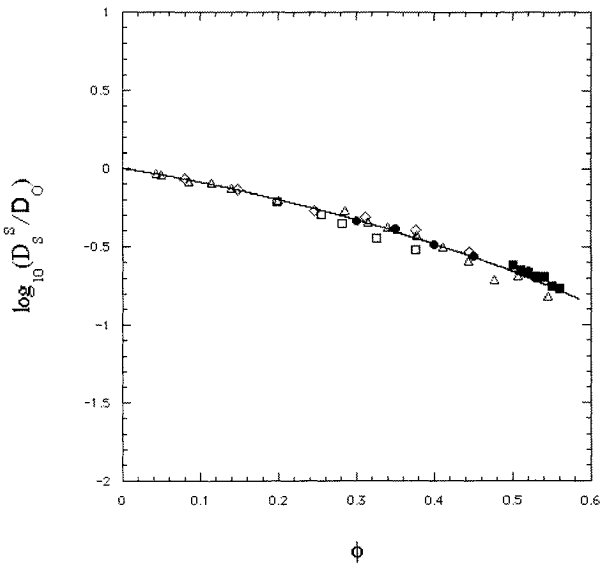

FIGURE 7. A log plot of the short-time self-diffusion coefficient $D_S^S(\phi)$ versus ϕ. The solid line indicates the theoretical short-time self-diffusion coefficient $D_S^S(\phi)$ given by Eq. (8). The filled symbols indicate the simulation results given by $[D_S^{L(A)}/d_0]/[D_S^{L(C)}/D_0]$; the circles for a monodisperse case and squares for a polydisperse case. Shown are also the experimental data from Ref. [13] (squares), Ref. [14] (triangles), and Ref. [15] (diamonds).

the theoretical and experimental results very well within errors for a wide range of volume fractions. Hence the following relation holds:

$$\frac{D_S^{L(A)}(\phi_{eq})}{d_0} = \frac{D_S^S(\phi_{eq})}{D_0}\frac{D_S^{L(C)}(\phi_{eq})}{D_0}. \qquad (38)$$

CONCLUSION

In this paper, we have tested whether the long-time collective behavior is universal or not by performing two types of computer simulations on hard-sphere systems, BD on colloidal suspensions and MD on atomic systems. Thus, we have shown in both systems that the many-body collision interactions lead to the same singular behavior of the long-time self-diffusion coefficient as that obtained by the many-body hydrodynamic interactions, except that the singular points are modified.

Next, we point out that two types of hydrodynamic interactions are necessary to recover the theoretical result given by Eq.(12). One is the short-time (uncorrelated) hydrodynamic inetractions, leading to D_S^S. Then, $D_S^{L(C)}$ reduces to $D_S^{L(A)}$. The other is the long-time (correlated) hydrodynamic interactions. This effect must shift the singular point $\phi_c \simeq 0.586$ to ϕ_g^{TO}. Thus, $D_S^{L(A)}$ may finally reduce to D_S^L. Finally, the diffusion coefficient similar to Eq.(31) also holds for magnetic colloids, where the dipole interactions play an important role. This will be discussed elsewhere.

ACKNOWLEDGMENTS

This work was partially supported by Grants-in-aid for Science Research with No. 14540348 from Ministry of Education, Culture, Sports, Science and Technology of Japan. Numrical computations for this work were performed on the ORIGIN 2000 machine at the Institute of Fluid Science, Tohoku University.

REFERENCES

1. M. Tokuyama and I. Oppenheim, Phys. Rev. E **50**, R16-R19 (1994).
2. M. Tokuyama and I. Oppenheim, Physica A **216**, 85-119 (1995).
3. M. Tokuyama, Physica A **102**, 399-430 (1980); **109**, 128-160 (1981).
4. M. Tokuyama, Physica A **294**, 23-43 (2001).
5. M. Tokuyama, Y. Enomoto, and I. Oppenheim, Physica A **270**, 380-402 (1999).
6. W. van Megen, T. C. Mortensen, S. R. Williams, J. Müler, Phys. Rev. E **58**, 6073-6085 (1998).
7. P. N. Segrè and P. N. Pusey, Phys. Rev. Lett. **77**, 771-774 (1996).
8. M. Tokuyama, Physica A **289**, 57-85 (2001).
9. M. Tokuyama, H. Yamazaki, and Y. Terada, Phy. Rev. E **67**, 062403 (2003).
10. M. Tokuyama, H. Yamazaki, and Y. Terada, Physica A **328**, 367-379 (2003).
11. W. S. Jodrey and E. M. Tory, Phys. Rev. A **32**, 2347-2351 (1985).
12. B. Doliwa and A. Heuer, Phys. Rev. E **61**, 6898-6908 (2000).
13. P.N. Pusey and W. van Megen, Nature (London) **320**, 340-342 (1986).
14. R. H. Ottewill and N. S. J. Williams, Nature **325**, 232-234 (1987).
15. A. van Veluwen and H. N. W. Lekkerkerker, Phys. Rev. A **38**, 3758-3763 (1988).